ELSEVIER

0958-9465(94)00028-X

Cement & Concrete Composites **17** (1995) 135–145

0958-9465/95/$9.50

Simulation of Fracture in Cement-Based Composites

J. Bolander Jr & H. Hikosaka

Department of Civil Engineering, Kyushu University, Fukuoka 812, Japan

(Received 2 June 1993; accepted 22 September 1993)

Abstract

A nonlocal smeared-cracking finite element model is used to simulate tensile fracture in mortar notched-beam specimens. The nonlocal model resolves the distributions of damage and energy consumption within the fracture process zone, as well as accounts for variance in fracture energy along the ligament length. Results correlate well to experimental and analytical results given by other researchers for fracture over the central portion of the ligament. However, standard nonlocal averaging causes excess energy consumption in regions subjected to high strain gradients. To promote natural fracture development and realistic energy consumption near the pre-notch tip, the nonlocal averaging process is modified in this vicinity.

Keywords: Concrete fracture, nonlocal modeling, fracture energy, size effect.

INTRODUCTION

Conventional finite element models for concrete cracking ignore the details of the fracture process, but rather use macroscopic notions of stress vs crack opening (discrete models[1]) or stress vs crack strain (continuum models[2]) to describe fracture. In both cases, direct tensile strength, the shape of the softening relation and fracture energy are important parameters for obtaining accurate results in fracture-sensitive situations. Since their conception these conventional models have been applied, with reasonable success, to a variety of structural analysis problems.

In recent years, there has been growing interest in numerically modeling the microbehavior of the fracture process, including estimating fracture process zone (FPZ) size and the distribution of strain, damage and energy consumption within its limits. Efforts in this direction are necessary for engineering more efficient cement-based materials and for improving analysis capabilities. Advances in experimental techniques related to FPZ measurements[3–10] are providing the necessary means for verifying new models. Insight into the micromechanics of fracture is also helping to progress related areas of research, such as the assessment of material performance under extreme environmental conditions.

By discretely modeling the basic components at the meso-structural level (i.e. cement matrix, aggregate inclusions and interfacial zones)[11–13] it is possible to simulate the essential features of concrete fracture, including the localization process which accompanies fracture. However, such approaches are computationally demanding and some of the input parameters needed at the component level are difficult to determine, particularly for two-dimensional analyses.[12,14] It is therefore attractive to develop continuum theories which, by virtue of having micromechanical bases, likewise simulate the essential features of fracture.[15] Alternatively, the microstructure's role in limiting localization can be realized by embedding an internal length scale into a continuum description.[16,17] Several variant approaches have been proposed and such enhanced continuum theories may be separated into two classes:[17] (1) non-local or gradient continuum theories, and (2) theories which utilize the concept of micropolar continua. Models relying on such concepts have important advantages over conventional continuum models, which suffer from various deficiencies (most notably, an inability to describe the localization process).[16,18] Moreover, due to the macroscopic nature of many of the input parameters, enhanced continuum models possess

attractive features which may be difficult to obtain using detailed micromechanical descriptions.

In this paper, a nonlocal smeared-crack finite element procedure[19] is used to simulate tensile fracture in mortar notched-beam specimens. The basic concept of a nonlocal continuum is that stress at a point depends on a spatial average of strain over a representative volume surrounding the point.[16] The size of this volume has been related to some characteristic length l of the micro- (or meso-) structure of the material.

As a consequence of limiting localization, the nonlocal model gives multi-dimensional representations of the FPZ as it travels along the ligament length. Local stress–strain response and the distributions of damage and energy consumption within the FPZ are provided; an estimate of the energies consumed by the microcracking and bridging processes is also made. These results are compared with experimental and analytical results given by other researchers.

The nonlocal model places no direct restriction on FPZ size or the distribution of damage and, therefore, has some ability to simulate local variances in fracture energy, such as those which occur near the specimen boundaries.[20] Numerical results presented here, however, show that standard nonlocal averaging causes excess energy consumption in regions subjected to high strain gradient. (By 'standard averaging', we mean the characteristic length l is constant over the fracture domain.) It appears l is not strictly a material parameter, but also depends on the surrounding stress and strain fields and damage conditions. Another recent study has come to similar conclusions.[21] To promote natural fracture development and realistic energy consumption near the prenotch tip, we reduce l in this vicinity. The ensuing results correlate much better with experimental observations. That is, local fracture energy is smaller near the notch tip and increases until reaching a constant value through the mid-portion of the ligament. Such simulation of fracture energy variance is useful for investigating mechanisms causing size effect, i.e. the dependence of global specific fracture energy on specimen size and/or geometry.

NONLOCAL SMEARED-CRACK MODEL

The nonlocal smeared-crack model[19] is outlined to facilitate later discussions. For the case of plane stress, the local form of the stress–strain law (in crack-plane coordinates) is:

$$\begin{Bmatrix} \varepsilon_{11} \\ \varepsilon_{22} \\ \gamma_{12} \end{Bmatrix} = \begin{bmatrix} \frac{1}{E} & \frac{-\nu}{E} & 0 \\ \frac{-\nu}{E} & \frac{1}{E} & 0 \\ 0 & 0 & \frac{2(1+\nu)}{\beta E} \end{bmatrix} \begin{Bmatrix} \sigma_{11} \\ \sigma_{22} \\ \sigma_{12} \end{Bmatrix} + \begin{Bmatrix} \varepsilon^{f} \\ 0 \\ 0 \end{Bmatrix} \quad (1)$$

$$= \begin{bmatrix} \frac{1}{E(1-\omega)} & \frac{-\nu}{E} & 0 \\ \frac{-\nu}{E} & \frac{1}{E} & 0 \\ 0 & 0 & \frac{2(1+\nu)}{\beta E} \end{bmatrix} \begin{Bmatrix} \sigma_{11} \\ \sigma_{22} \\ \sigma_{12} \end{Bmatrix} \quad (2)$$

where E is Young's modulus, ν is Poisson's ratio, ε^{f} is the fracture strain and β is the shear retention factor for representing aggregate interlocking. The values σ_{11}, σ_{22}, σ_{12} and ε_{11}, ε_{22}, γ_{12} are the stresses and strains, respectively, with direction 1 being normal to the cracking plane. ω represents the degree of damage and varies from $\omega = 0$ (no damage) to $\omega = 1$ (complete damage). Increasing ω has the effect of increasing material compliance in the direction normal to the cracking plane.

For a model based on local strain, ω is adjusted so that stress normal to the cracking plane is released as shown by Fig. 1(a).

$$\varepsilon_{11} < \varepsilon_t: \quad \omega = 0$$

$$\varepsilon_{11} \geq \varepsilon_t: \quad \omega = f(\varepsilon_{11}) = 1 - \frac{f_t}{E\varepsilon_{11}} \exp\left[\frac{a}{\varepsilon_0}(\varepsilon_{11} - \varepsilon_t)\right] \quad (3)$$

where ε_t and f_t are the strain and stress, respectively, which correspond to crack initiation; ε_0 is a fracture strain associated with virtually zero crack-normal stress. Parameter a adjusts the degree of exponental softening; we have set $a = -5$ to approximate the global strain softening witnessed in direct tension testing.[22]

Nonlocal damage is defined using the same relations as in eqn (3) except nonlocal strain $\bar{\varepsilon}_{11}$ is considered instead of local strain ε_{11}. That is, $\bar{\omega} = f(\bar{\varepsilon}_{11})$, where the overbar is used to indicate

nonlocal variables; $\bar{\omega}$ then replaces ω in eqn (2). Note that only damage is treated as nonlocal, while the other state variables remain local in character.

Referring to Fig. 2, nonlocal strain is defined as a spatial weighted average of local strains over the continuum volume:

$$\bar{\varepsilon}_{11}(\mathbf{x}) = \frac{1}{V_r(\mathbf{x})} \int_V \alpha(\mathbf{s}-\mathbf{x}) \langle \varepsilon_{11}(\mathbf{s}) \rangle \, \mathrm{d}V \qquad (4)$$

where

$$V_r(\mathbf{x}) = \int_V \alpha(\mathbf{s}-\mathbf{x}) \, \mathrm{d}V \qquad (5)$$

$$\alpha(\mathbf{s}-\mathbf{x}) = \exp\left[-\left(\frac{2|\mathbf{s}-\mathbf{x}|}{l} \right)^2 \right] \qquad (6)$$

V is the volume of the entire continuum; α is an empirical weighting function (given the form of a 2-D normal distribution here); and l is the internal characteristic length. The pointed brackets $\langle\rangle$ denote treating only positive values of a variable (i.e. for $\varepsilon_{11} < 0 : \langle \varepsilon_{11} \rangle = 0$). During finite element computations, the integrals in eqns (4) and (5) are evaluated by summing discrete values over the element sampling points. Boundary conditions are dealt with approximately by simply deleting regions outside the continuum from the averaging process.

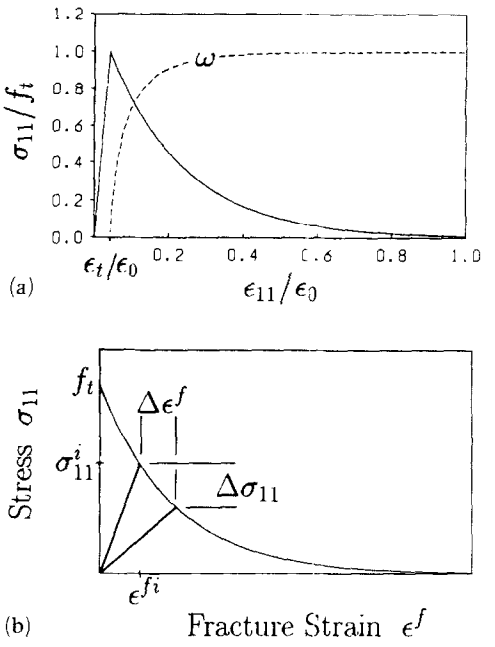

Fig. 1. Stress–strain relation normal to crack: (a) exponential softening model; (b) incremental energy consumption.

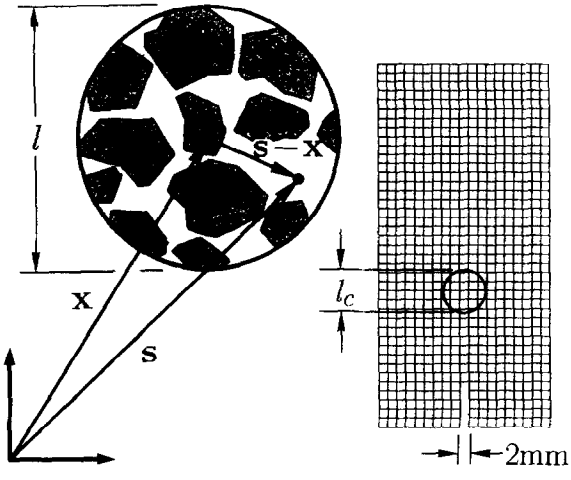

Fig. 2. Damage-representative volume and its relation to mesh size.

TEST SPECIMENS AND FINITE ELEMENT MODEL

Several series of mortar notched-beam specimens were tested in a separate study, as reported in Ref. 4. The specimen considered here is representative of one of the test series, which had dimensions and boundary conditions as shown in Fig. 3(a).

This test series indicated a fracture energy $g_f = 53$ J m^{-2} for cracks advancing through the center portion of the ligament. Lower case is used here to differentiate this 'steady-state' value from global specific fracture energy G_f as determined from standard tests.[23] The mortar used in the specimens had a maximum aggregate size $d_a \approx 3$ mm. Other pertinent parameters were taken from direct tension testing of a similar mortar: direct tensile strength $f_t = 4{\cdot}5 \pm 0{\cdot}5$ MPa; and Young's modulus $E = 27\,800 \pm 600$ MPa.

The finite element idealization of the test specimen and boundary conditions is shown in Fig. 3(b). Four-node quadrilateral elements composed of four constant strain triangular (CST) elements are used. The pre-notch is modeled by a one-element wide (i.e. 2 mm) gap at midspan. Characteristic length l is set equal to $l_c = 3d_a$, considering representative values given elsewhere.[2,24] Here, l_c represents a constant value used over the whole domain (Fig. 2) during initial computations. Later in this paper, l is varied near the notch tip so as to promote natural fracture development in that vicinity.

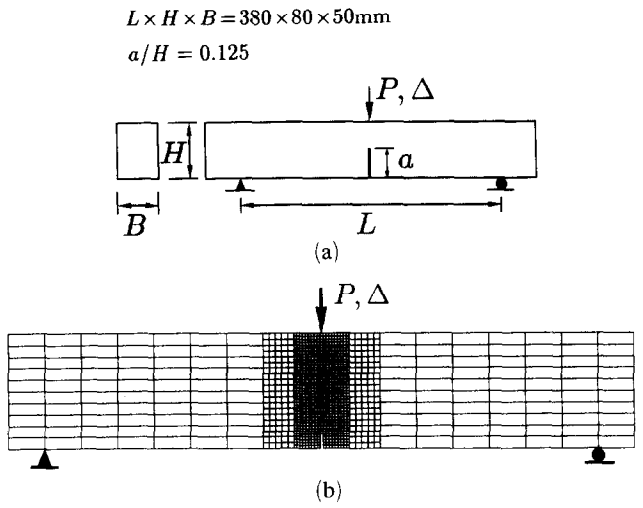

Fig. 3. Mortar notched-beam specimen: (a) test specimen dimensions; (b) finite element idealization.

FRACTURE PROCESS CHARACTERIZATION

Local stress–strain relations

Typical stress–strain response within the center portion of the ligament is shown in Fig. 4(a). As a consequence of nonlocal averaging, the local stress–strain relations no longer follow the model diagram shown in Fig. 1(a). Rather, sampling points incur varying degrees of damage depending on their location relative to the center of the process zone. Points near the center of the zone continue to load, consume the most energy, and eventually reach a completely damaged state, modeling material separation. Points to the sides unload sooner and consume progressively less energy with increasing distance from the center of the zone. Sampling Points 5 and 6 (responses not plotted) also become damaged and consume minor amounts of energy.

Due to strain concentration near the notch top, nonlocal strains computed for Sampling Point 1′ (Fig. 4(b)) are significantly less than the corresponding local strain at the same point. Since nonlocal damage $\bar{\omega}$, and consequently stress release normal to the crack plane, is controlled by nonlocal strain, the resulting local stress–strain relation greatly overestimates strength and energy capacity (Curve 1′). After crack advance, closing stresses behind the damage front reduce the degree of singularity acting at the damage front. Therefore, the difference between nonlocal and local strain measures (at yet undamaged sampling points) decreases over a certain distance from the notch tip. Thus, damage initiates near f_t from Sampling Point 4′ onward.

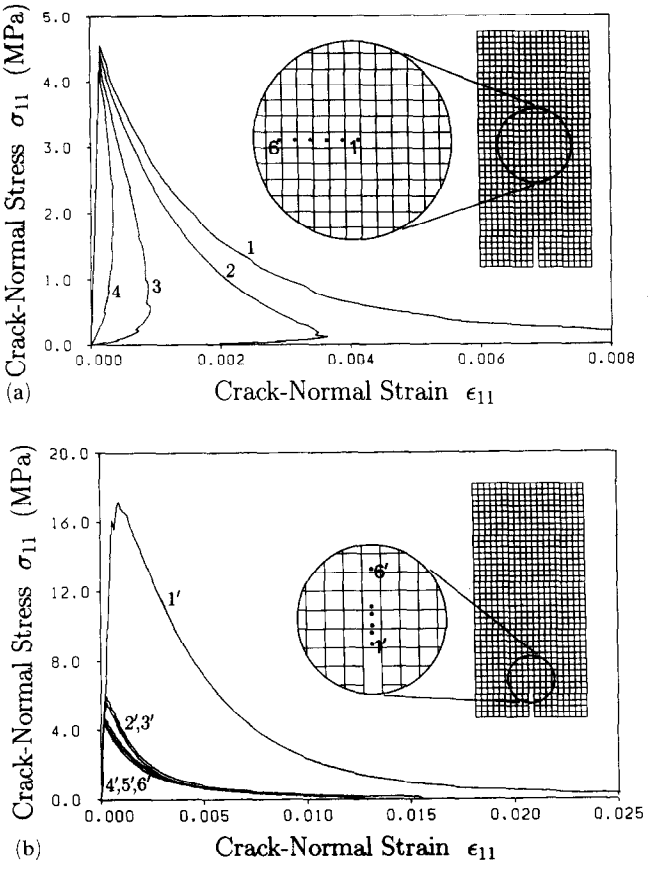

Fig. 4. Local stress–strain response: (a) through midportion of ligament; (b) near notch tip.

Fracture strain distribution

From eqns (1) and (2) the following expression can be obtained for fracture strain:

$$\varepsilon^f = \frac{\bar{\omega}}{1-\bar{\omega}} \frac{\sigma_{11}}{E} \tag{7}$$

Figure 5(a) shows the distribution of fracture strain within the densely meshed region for computed Stages I–V. The length of each line, centered at a particular sampling point, indicates the magnitude of fracture strain at that location; line orientation indicates crack-plane direction. To follow fracture strain development at lower load levels, these results have been normalized at each load step. A small dot, centered at a particular sampling point, indicates unloading at that location.

Fracture strain profiles, given in Fig. 5(b), show the response at section X–X for each stage. The width of the FPZ extends over many elements and fracture strains are initially rather uniformly distributed. However, with continued loading the fracture strains near the center of the band con-

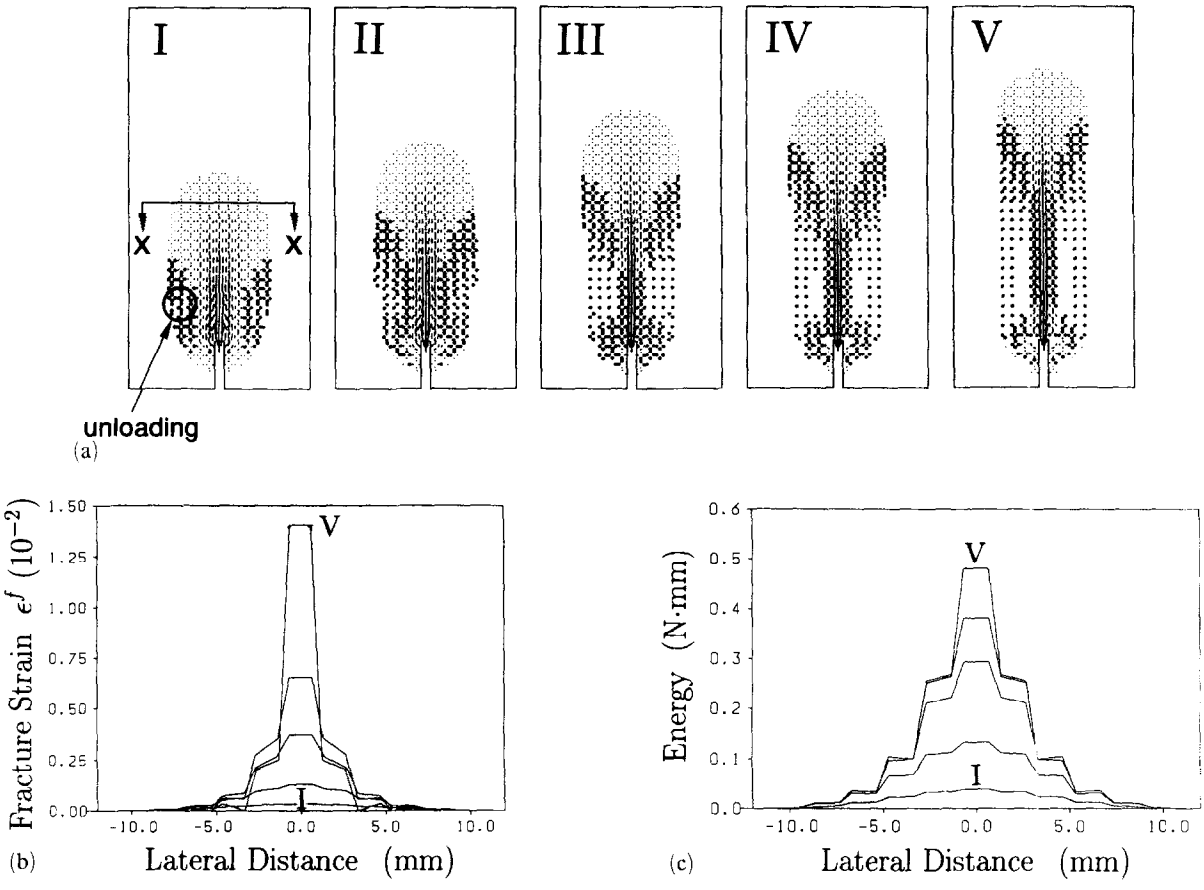

Fig. 5. Local response at section X–X: (a) fracture strain distributions; (b) fracture strain profiles; (c) energy profiles.

tinue to increase, while the sampling points to the sides show unloading behaviour.

Cedolin *et al.*[3] have used laser Moiré interferometry to obtain high-resolution measurements of strain variance in the vicinity of the FPZ. Similar to the behavior shown in Figs 5(a) and 5(b), strain fields measured experimentally indicate a broad zone of distributed microcracking which propagates in front of a discrete crack; unloading occurs to the sides of the developing crack. Fracture strain development in the numerical model (Fig. 5(b)) resembles that of corresponding total strain profiles given in Ref. 3. We would like to provide careful, quantitative comparisons with these and other recent experimental results, such as those obtained using laser moiré interferometry,[6] holographic interferometry,[7] and the laser speckle technique.[9] Before doing so, however, the differences between (1) such surface-type measurements, (2) the three-dimensionality of the actual fracture process[8] and (3) the results from two-dimensional analysis models should be better resolved. It should be emphasized that the numerical results are strongly dependent on the assumed characteristic length l. Reducing l, while holding all other inputs constant, has the effect of reducing the extent and energy absorbing capacity of the FPZ.

Fracture energy distribution

Using a secant model for unloading (Fig. 1(b)) the incremental specific energy consumed at a given sampling point can be approximated using:

$$\Delta\phi = \frac{1}{2}(\sigma_{11}^{i}\Delta\varepsilon^{f} - \varepsilon^{fi}\Delta\sigma_{11}) \tag{8}$$

Summing the incremental energies (i.e. $\Delta\phi$ times the appropriate tributary material volume) gives the energy consumed by the sampling point. Energy profiles made from the points along section X–X are shown in Fig. 5(c). As the fracture process travels through the section, the energy profile gradually increases and eventually reaches a limiting state as the fracture process passes completely through. Profiles computed at other sections over the center portion of ligament are nearly identical in shape and size.

The distribution of energy consumed by fracture is not just of academic interest, but is an

important characterization of material response and useful in the engineering of new high-performance cement-based materials.[25] Concrete fracture energy g_f may be separated into two components: (1) g_f' the energy consumed by peripheral microcracking, and (2) g_f'' the energy consumed by bridging mechanisms, such as frictional pullout and internal ligament bending, active during material separation. Based on experimental results, Cedolin *et al.*[3] estimated the ratio g_f'/g_f to be about 5%. Nirmalendran and Horii[26] developed an analytical approach which treats microcracking and bridging separately; they show that g_f'/g_f ranges between 1 and 4%, depending on the length of the bridging zone. Planas *et al.*[27] used elasto-plastic numerical computations to estimate g_f'/g_f to be about 1–2% for normal size specimens; they found an upper bound of this ratio to be less than 5% by analysing steady cohesive crack growth in an infinite medium. Bolander *et al.*[14] used a lattice model to simulate fracture in a series of concrete specimens. From their results g_f'/g_f is found to be less than 3%.

While the nonlocal model described in this paper makes no distinction between the various mechanisms which underlie fracture, from Figs 4(a) and 5(c) it is clear that most of the fracture energy is consumed near the center of the FPZ. Rather than thinking strictly in terms of a crack-plane, material separation takes place over a finite width in continuum models. Assuming the mechanisms leading to material separation occur over the characteristic length $l = 3d_a$, then g_f'/g_f is about 12%. In light of the above estimates for g_f'/g_f, which range between 1 and 5%, the energy distribution predicted here appears to be too gentle. Moreover, some studies[6,8,14] indicate that the process of material separation occurs over a smaller width of about $1d_a$. Further research is necessary for correlating the numerical results with these and other aspects of the crack-local response. In particular, experience with this basic model suggests that the fundamental mechanisms composing fracture need better representation in the numerical formulation.

VARIANCE IN FPZ SIZE AND ENERGY CONSUMPTION

Experimental observations

Specific fracture energy G_f is often regarded as a constant for purposes of numerical calculation, yet numerous tests have shown its value varies with specimen size and geometry.[28] This size/geometry dependence, or 'size effect', is caused by many factors.[29,30] When testing bend-type specimens, one such factor is that FPZ size and energy consumption vary along the ligament length due to boundary effects.[20] That is, the FPZ grows from the notch tip, reaches a near constant size over the center portion of the ligament (if the specimen is sufficiently large) and then becomes smaller under the influences of increased strain gradient and confinement when approaching the compression face of the specimen. There are related changes in the energy demands for driving the fracture process as well. For longer ligament lengths these boundary effects have less influence on the global specific fracture energy and, thus, there is a size effect mechanism.

Other experimental results also indicate dependence of the fracture process on the surrounding stress and strain fields. Bascoul *et al.*[31] initiated microfracture under a wide range of strain gradients and found that the density of stable microcracks is strongly dependent on strain gradient, higher gradients leading to higher concentrations of damage. Mihashi and Nomura[10] used AE measurements to show that the fracture process grows out from a notch tip in normal concrete and they correlated the width of the FPZ with critical crack opening displacement in fictitious crack models. Slowik and Wittmann[32] have determined that fracture energy depends on strain gradient, with higher gradients leading to lower fracture energies.

Reducing characteristic length l near the notch tip

One of the great advantages of using enhanced continuum models is that the FPZ is freer to vary along the ligament length, irrespective of mesh size and orientation. It follows that local variance in fracture energy should be accounted for as well. However, as shown in Fig. 4(b), standard nonlocal averaging grossly overestimates strength and energy consumption near the notch tip. It appears that some of the nonlocal parameters should vary to account for the changing nature of fracture under high strain gradients.

To promote proper energy consumption near the notch tip, the nonlocal averaging process is modified *a priori*, as shown in Fig. 6. The characteristic length l, set equal to l_c in the preceding computations, is gradually reduced to a length l^* when approaching the notch tip from any given radial direction. This has physical meaning since,

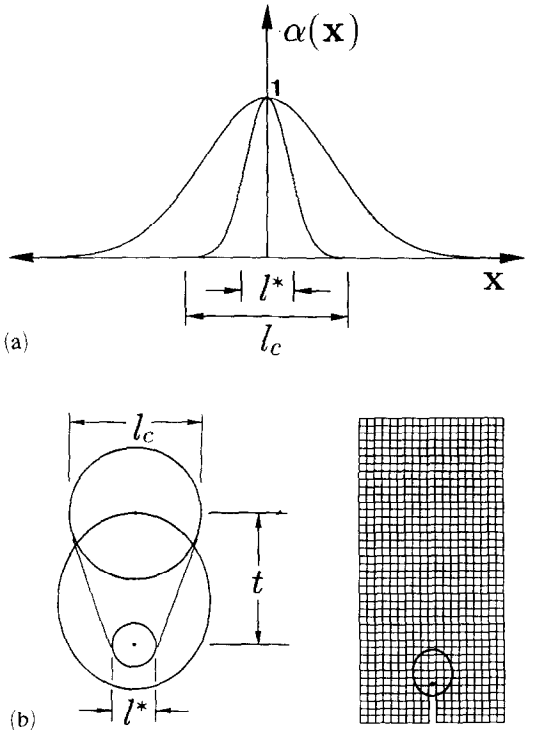

Fig. 6. Reducing characteristic length l near the notch tip: (a) 1-D normal distribution; (b) transition region around notch tip.

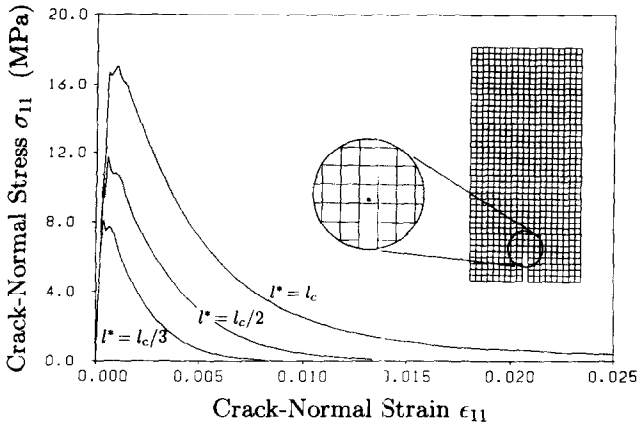

Fig. 7. Local stress–strain response just above notch tip obtained from various averaging schemes.

near a notch tip, the highly stressed volume where the FPZ forms and fracture initiates is likely to be smaller than during subsequent fracture when closing stresses behind the fracture front reduce the degree of singularity acting at the front. An ellipse is used to define the limits within which l is contracted; the integration point just above the notch tip coincides with the ellipse's focal point, as shown in the figure. The elliptical shape is chosen merely because of its simplicity and in order to bias the transition region in the direction of fracture propagation.

Reducing l^*, while keeping the transition length t constant, decreases the strength and energy absorbing capacity of the material surrounding the notch tip, particularly just above the tip (Fig. 7). For $l^* = l_c/3$ the peak stress is still rather high, reaching almost $2f_t$, but this may be reasonable for a small volume under high strain.[33] In the following analyses, where modified averaging is used, l^* and t are set to $l_c/3$ and l_c, respectively. Of course, these values are probably not adequate for general application (i.e. for situations of differing geometry, material properties and finite element idealization). A procedure should be developed for modifying the characteristic length and/or other parameters in the nonlocal setting, as the fracture process evolves during computations.

Simulation of fracture process variance

Figure 8 shows contours of energy consumption rate obtained by both standard ($l^* = l_c$) and modified ($l^* = l_c/3$) averaging near the notch tip. Both planar contours (normalized within each load step) and perspective view contours (energy per unit displacement at the load point) are given. Load stages correspond to prescribed displacement values, as indicated in Fig. 9. Results from standard averaging show an excess amount of energy being consumed near the notch tip; this not only inhibits natural process zone formation, but also causes the global load-deflection response to be too strong. On the other hand, modified averaging promotes natural process zone formation. That is, after peak load the process zone detaches from the notch tip and thereafter becomes nearly constant in size. Despite these differences near the notch tip, both approaches give essentially the same results for fracture over the mid-portion of the ligament. Figures 4(a) and 5 represent the results of both approaches equally well.

Reducing l near the notch tip also improves the quantitative simulation of energy consumption during crack propagation. Figure 10(a) compares the numerical results obtained from modified averaging with test series data. Each • mark represents the results for one test specimen, as described in Ref. 4, and the dashed line indicates a sort of best fit to these data points. The damage front associated with $\bar{\omega} = 0{\cdot}99$ is used to define effective crack length in the numerical model (Fig. 10(b)). Energy consumption in the numerical model is computed by summing the individual sampling point energies. Energy consumption rate $g_f(\eta)$ could be calculated from the slope of the results given in Fig. 10(a), where η is the distance

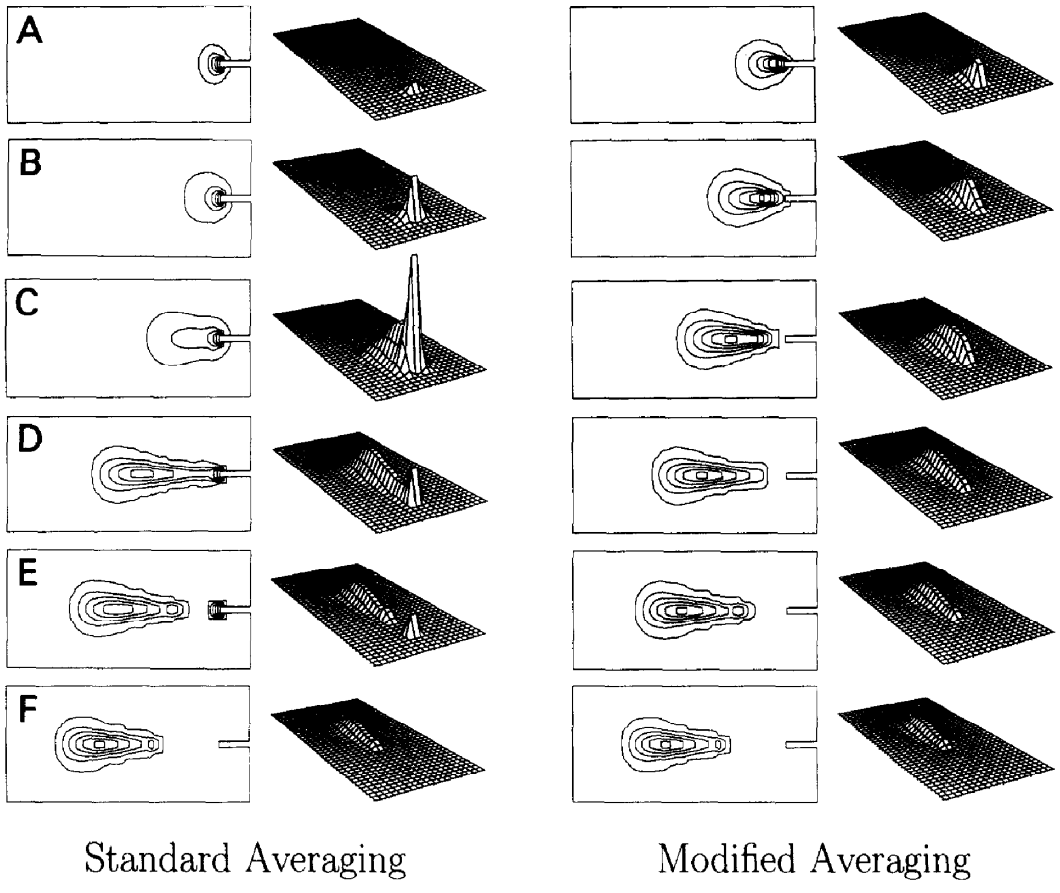

Fig. 8. Smoothed energy consumption rate.

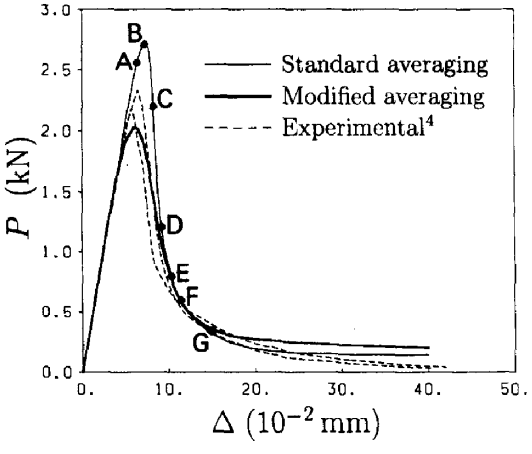

Fig. 9. Reactive force vs controlled displacement.

from the notch tip along the ligament length. The numerical results agree well with the experimental data, particularly with respect to: (1) initial energy consumption prior to crack formation, (2) lower energy consumption rate just after crack formation, and (3) nearly constant energy consumption rate over the ligament mid-length. Effective crack lengths defined by the traction free condition $\bar{\omega} = 1{\cdot}00$ provide results similar to those shown in Fig. 10(a), except the energy values are increased by about 0·015 J. Results from the standard averaging procedure have not been plotted in Fig. 10(a) due to difficulties in defining the numerical crack. When using standard averaging, the FPZ does not detach from the notch tip until late in the loading history (near stage E, shown in Fig. 8). Accordingly, roughly 50% of the total fracture energy is consumed prior to effective crack initiation.

The variable $g_f(\eta)$ determined in the above manner directly relates energy consumption to crack advance. However, when fracture does not proceed in a steady-state manner, it is not clear how to differentiate the energy necessary for crack advance and the energy associated with changes in the process zone itself. There is also the question of how to define a numerical crack. For investigating the conditions near the notch tip, where these concerns are particularly relevant, it is instructive to define:

$$g_f(\eta) = \int_{-\infty}^{\infty} \phi(\eta, \xi)\, d\xi \tag{9}$$

where $\phi(\eta, \xi)$ is the spatial distribution of energy consumption per unit volume projected on the

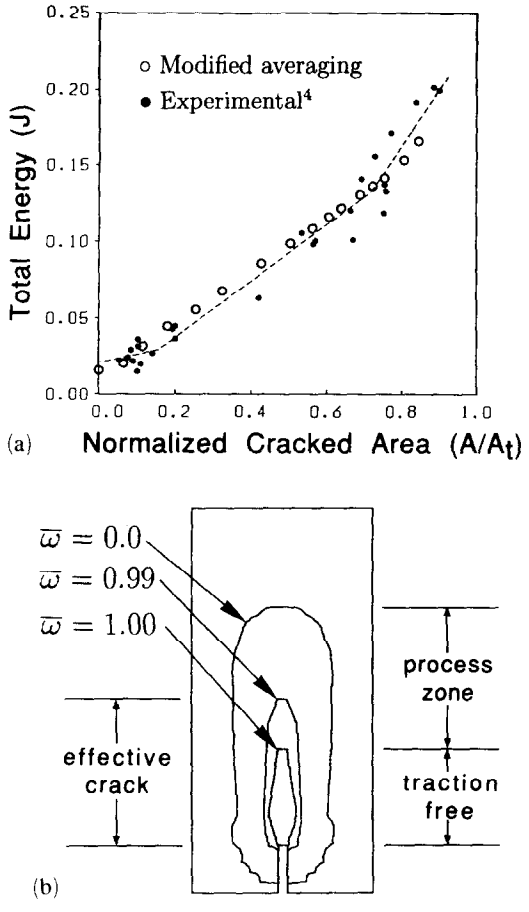

Fig. 10. Energy rate variance obtained from modified averaging scheme: (a) global energy consumption vs cracked area; (b) nonlocal damage contours.

η-ξ plane, ξ being the direction transverse to crack advance. During finite element computations the specific energy attributed to each sampling point is obtained via eqn (8); multiplying these values by the appropriate tributary volume and then summing along each transverse row of elements gives discrete values of $g_f(\eta)$ along the ligament length. Figure 11 shows $g_f(\eta)/g_f$ computed up through load stage G indicated in Figs 8 and 9. By this stage, the traction free condition has extended up to about $\eta/\eta_{lig} = 0{\cdot}5$, where η_{lig} is the ligament length. Again, standard averaging provides unacceptable results near the notch tip; modified averaging provides much more realistic energy variance in this vicinity. Both standard and modified averagings give virtually the same results over the mid-portion of the ligament and match the experimental value well. This is one of the main requirements of the model and the value of ε_0 in eqn (3) was adjusted for this purpose. For $\eta/\eta_{lig} > 0{\cdot}5$, the fracture process is still active and therefore $g_f(\eta)/g_f$ drops off sharply. Unfortunately, there is currently no experimental technique available to measure the spatial distribution of energy consumption due to fracture. However, the variation of fracture energy obtained from modified averaging, shown in Fig. 11, is quite similar to experimental findings[34] which used load-displacement measurements to compute energy consumption and a compliance method to estimate crack advance.

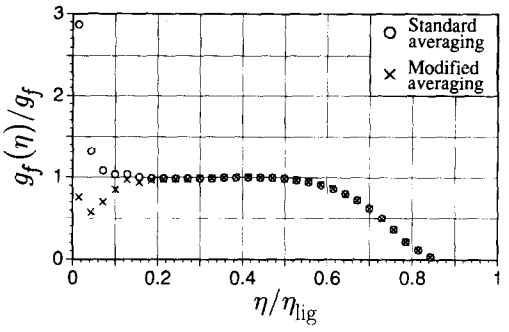

Fig. 11. Fracture energy variance along ligament length.

CONCLUSIONS

Conventional continuum models for concrete cracking provide almost no meaningful information concerning crack-local response. Indeed, such information should be pursued using micromechanical analyses. By introducing an internal length scale into a continuum description, however, the microstructure's role in limiting localization is practically realized. These so-called enhanced continuum models have received much attention in recent years. Many important consequences arise from limiting localization, one being that fracture is freer to develop irrespective of mesh size and orientation. This opens up new possibilities for analysing fracture. Here, for example, a nonlocal smeared-cracking approach[19] is used to investigate the effects of strain gradient on FPZ size and energy consumption rate. Though conceptually simple, this nonlocal model also reproduces many of the essential features of fracture in cement-based composites, as shown through comparisons with various experimental and analytical results. In addition, computed distributions of damage and fracture energy are used to clarify some basic issues concerning the nonlocal modeling of fracture in such materials. The findings presented in this paper include:

(1) A broad zone of damage forms in front of a developing crack. Damage is initially rather uniformly distributed and then localizes

into a much narrower band modeling an actual crack; unloading occurs to the sides of the developing crack.

(2) Local stress–strain response does not follow the prescribed stress–strain diagram and varies depending upon sampling point location within the FPZ. While the numerical model makes no distinction between the various mechanisms which underlie fracture, we can infer that peripheral 'microcracking' consumes relatively little energy compared to the mechanisms involved in material separation.

(3) FPZ size and energy consumption rate are nearly constant over the central portion of the ligament (away from the boundary effects). This steady-state energy consumption rate can be tuned to match experimental results well.

(4) FPZ size and energy consumption rate vary near the notch tip due to the influences of strain gradient on the fracture process. Moreover, it appears that characteristic length l is not strictly a material parameter, as previously believed, but also depends on the surrounding stress and strain fields and damage conditions. To promote natural fracture development near the notch tip, we have reduced l in this vicinity. This variance of l was set prior to computation; different materials, geometries, or finite element idealizations would require different settings. For general application, a procedure is necessary for modifying the characteristic length (and/or other parameters in the nonlocal setting) as the fracture process evolves during computations.

(5) By accounting for local variances in fracture energy, the nonlocal model is useful for studying mechanisms causing the dependence of specific fracture energy on specimen size and/or geometry.

(6) Simplicity and reliance on macroscopic parameters are attractive features when simulating the global response (e.g. steady-state energy consumption rate) is a primary concern. However, shortcomings of this basic model become apparent when investigating the results for crack-local response. Along with the need to address the three-dimensionality of the material and fracture process, this formulation should be developed to better represent the fundamental mechanisms composing fracture.

ACKNOWLEDGEMENTS

This research has been partially supported through a Grant-in-Aid for Scientific Research from the Japanese Ministry of Education, Science and Culture.

REFERENCES

1. Hillerborg, A., Modeer, M. & Petersson, P.-E., Analysis of crack formation and crack growth in concrete by means of fracture mechanics and finite elements. *Cement & Concrete Res.*, **6** (1976) 773–82.
2. Bažant, Z. P. & Oh, B. Y., Crack band theory for fracture of concrete. *Mater. Struct.*, **16** (1983) 155–77.
3. Cedolin, L., Dei Poli, S. & Iori, I., Tensile behavior of concrete. *J. Eng. Mech. Div., ASCE*, **113** (3) (1987) 431–49.
4. Bascoul, A., Kharchi, F. & Maso, J. C., Concerning the measurement of the fracture energy of a micro-concrete according to the crack growth in a three point bending test on notched beams. In *SEM/RILEM Int. Conf. on Fracture of Concrete and Rock*, ed. S. P. Shah & S. E. Swartz. Springer-Verlag, New York, 1987, pp. 396–408.
5. Maji, A. K. & Shah, S. P., Process zone and acoustic emission measurements in concrete. *Exp. Mech.*, **27** (1988) 27–33.
6. Du, J. J., Kobayashi, A. S. & Hawkins, N. M., An experimental-numerical analysis of fracture process zone in concrete fracture specimens. *Engng Fracture Mech.*, **35** (1–3) (1990) 15–27.
7. Castro-Montero, A., Shah, S. P. & Miller, R. A., Strain field measurement in fracture process zone. *J. Eng. Mech., ASCE*, **116** (11) (1990) 2463–84.
8. van Mier, J. G. M., Mode I fracture of concrete: discontinuous crack growth and crack interface grain bridging. *Cement & Concrete Res.*, **21** (1991) 1–15.
9. Horii, H. & Ichinomiya, T., Observation of fracture process zone by laser speckle technique and governing mechanism in fracture of concrete. *Int. J. Fracture*, **51** (1991) 19–29.
10. Mihashi, H. & Nomura, N., Microcracking and tension-softening properties of concrete. *Cement & Concrete Composites*, **14** (1992) 91–103.
11. Roelfstra, P. E., Sadouki, H. & Wittmann, F. H., Le béton numérique. *Mat. & Constr.*, **107** (1985) 327–35.
12. Roelfstra, P. E., Simulation of strain localization processes with numerical concrete. In *Cracking and Damage — Strain Localization and Size Effect*, eds J. Mazars & Z. P. Bažant. Elsevier Applied Science, London, 1989, pp. 79–90.
13. Schlangen, E. & van Mier, J. G. M., Experimental and numerical analysis of micromechanisms of fracture of cement-based composites. *Cement & Concrete Composites*, **14** (1992) 105–18.
14. Bolander, J., Hikosaka, H. & Shiraishi, T., Effects of strain gradient on concrete tensile fracture. In *Memoirs of the Faculty of Engineering*, Vol. 53. Kyushu University, Fukuoka, Japan, 1993, pp. 103–19.
15. Okui, Y., Horii, H. & Akiyama, N., A continuum theory for solids containing microstructures. *Int. J. Engng Sci.*, **31** (5) (1993) 735–49.
16. Bažant, Z. P., Mechanics of distributed cracking. *Appl. Mech. Rev., ASME*, **39** (5) (1986) 675–705.
17. de Borst, R. & Mühlhaus, H. B., Continuum models for discontinuous media. In *Fracture Process in Concrete, Rock and Ceramics*, eds J. G. M. van Mier, J. G. Rots &

A. Baker. Spon/Chapman & Hall, London, 1991, pp. 601–18.
18. Rots, J. G. & Blaauwendraad, J., Crack models for concrete: discrete or smeared? Fixed, multi-directional or rotating? *HERON*, **34** (1) (1989) 1–59.
19. Bažant, Z. P. & Lin, F. B., Nonlocal smeared cracking model for concrete fracture. *J. Struct. Div., ASCE*, **114** (11) (1988) 2493–510.
20. Hu, X.-Z. & Wittmann, F. H., Fracture energy and fracture process zone. *Mater. Struct.*, **25** (149) (1992) 319–26.
21. Ožbolt, J., General microplane model for concrete. In *Numerical Methods in Fracture Mechanics of Concrete*, ed. F. H. Wittmann. A. A. Balkema Publishers, Rotterdam, The Netherlands, 1993, pp. 173–87.
22. Reinhardt, H. W. & Cornelissen, H. A. W., Post-peak cyclic behaviour of concrete in uniaxial tension and alternating tensile and compressive loading. *Cement & Concrete Res.*, **14** (2) (1984) 263–70.
23. RILEM TC-50 FMC (Draft Recommendation), Determination of the fracture energy of mortar and concrete by means of three-point bend tests on notched beams. *Mater. Struct.*, **18** (106) (1985) 285–90.
24. Bažant, Z. P. & Pijaudier-Cabot, G., Measurement of characteristic length of nonlocal continuum. *J. Engng Mech., ASCE*, **115** (4) (1989) 755–67.
25. Li, V. C. & Hashida, T., Ductile fracture in cementitious materials? In *Fracture Mechanics of Concrete Structures*, ed. Z. P. Bažant. Elsevier Science Publishers Ltd, Essex, England, 1992, pp. 526–35.
26. Nirmalendran, S. & Horii, H., Analytical modelling of microcracking and bridging in fracture of quasi-brittle materials. *J. Mech. Phys. Solids*, **40** (2) (1992) 863–86.
27. Planas, J., Elices, G. & Guinea, G. V., Measurement of the fracture energy using three-point bend tests: Part 2 — Influence of bulk energy dissipation. *Mater. Struct.*, **25** (149) (1992) 305–12.
28. Hillerborg, A., Results of three comparative test series for determining the fracture energy G_f of concrete. *Mater. Struct.*, **18** (1985) 33–9.
29. Fracture mechanics of concrete: concepts, models, and determination of material parameters. Report by ACI Committee 446 (Fracture Mechanics). In *Fracture Mechanics of Concrete Structures*, ed. Z. P. Bažant. Elsevier Science Publishers Ltd, Essex, England, 1992, pp. 1–140.
30. Guinea, G. V., Planas, J. & Elices, G., Measurement of the fracture energy using three-point bend tests: Part 1 — Influence of experimental procedures. *Mater. Struct.*, **25** (148) (1992) 212–18.
31. Bascoul, A., Ollivier, J. P. & Poushanchi, M., Stable microcracking of concrete subjected to tensile strain gradient. *Cement & Concrete Res.*, **19** (1989) 81–8.
32. Slowik, V. & Wittmann, F. H., Influence of strain gradient on fracture energy. In *Fracture Mechanics of Concrete Structures*, ed. Z. P. Bažant. Elsevier Science Publishers Ltd, Essex, England, 1992, pp. 424–9.
33. Bascoul, A. & Maso, J. C., Microcracking and cracking limit state as functions of strain gradients for concrete. *Cement & Concrete Res.*, **17** (1987) 661–72.
34. Brameshuber, W. & Hilsdorf, H. K., Influence of ligament length and stress state on fracture energy of concrete. *Engng Frac. Mech.*, **35** (1–3) (1990) 95–106.